

Topographic imaging of convoluted surface of live cells by scanning ion conductance microscopy in a standing approach mode

Yasufumi Takahashi,^a Yumi Murakami,^a Kuniaki Nagamine,^a Hitoshi Shiku,^a Shigeo Aoyagi,^b Tomoyuki Yasukawa,^c Makoto Kanzaki^d and Tomokazu Matsue^{*a}

Received 8th February 2010, Accepted 22nd April 2010

DOI: 10.1039/c002607g

Scanning ion conductance microscopy (SICM) using a nanopipette as a probe and ionic current as a feedback signal was introduced as a novel technique to study live cells in a physiological environment. To avoid contact between the pipette tip and cells during the conventional lateral scanning mode, we adopted a standing approach (STA) mode in which the probe was moved vertically to first approach and then retracted from the cell surface at each measurement point on an XY plane. The STA mode ensured non-contact imaging of the topography of live cells and for a wide range of uneven substrates ($500 \times 300 \mu\text{m}$ to $5 \times 5 \mu\text{m}$). We also used a field-programmable gate array (FPGA) board to enhance feedback distance regulation. FPGA dramatically increased the feedback speed and decreased the imaging time (450 s per image) with enhanced accuracy and quality of live cell images. To evaluate the potential of the STA mode for SICM, we carried out imaging of a convoluted surface of live cell in various scan ranges and estimated the spatial resolutions of these images.

Introduction

Scanning probe microscopy (SPM), particularly atomic force microscopy (AFM), has been applied for a variety of physical, chemical and structural characterizations of live cells. Considerable efforts have been made to improve the resolution and scan rate as well as to reduce the stress applied to live samples during imaging.^{1–3} However, conventional AFM requires physical contact comparable to a cantilever with the sample, which might induce undesirable morphological deformations, especially for measurements under water. Since the surfaces of live cells are too soft and water viscosity cannot be disregarded, introduction of the undesired effects on cell viability is unavoidable due to the force used as a feedback signal during AFM imaging. Non-contact oscillating AFM techniques for live cell imaging have been developed and are already available in commercial microscopes. However, the spatial resolutions of AFM images obtained for live cell samples are considerably inferior to those for fixed cells.

Among various SPMs, scanning ion conductance microscopy (SICM) is an effective tool for non-contact topographical imaging of live cells^{4–6} because measurements are performed under physiological conditions. SICM uses a micro- or nanopipette as a scanning probe to detect an ionic current between an electrode inside the pipette and an electrode located in a bath. The pipette–sample distance is regulated by the ionic

currents used as feedback signals. When the pipette approaches a sample surface, the resistance between the two electrodes increases and ionic current decreases. The magnitude of ionic current depends on the pipette–sample distance. Therefore, ionic current can be used as a feedback signal to maintain a constant pipette–sample distance.⁷

SICM provides information on the height of live cells by bringing the pipette tip within the proximity of the cell surface. SICM has previously been combined with other analytical tools including scanning near-field optical microscopy^{8–12} and confocal microscopy^{13–15} in order to simultaneously obtain high resolution fluorescent information and cell surface topography. SICM has also been used as a tool for the precise local delivery of various biomolecules based on electrophoresis.^{16–23} In addition, localized patch clamp using the SICM configuration^{24–26} and mapping ion channels²⁷ have been performed.

The scanning mode is a key element for measuring convoluted live cell surface topography because the feedback distance control system cannot predict height information in advance. Thus, a conventional scanning method in which the tip–sample distance is controlled by maintaining the set point of a feedback signal at a constant value can possibly deform a live cell surface and generate artifacts during the lateral motion of the tip. In particular, neurons are quite difficult to image because they have a narrow axon and large cell body. Jumping-mode AFM, the tip literally jumping from one image point to another, is effective for convoluted surface topography measurement of biological sample.²⁸ Scanning electrochemical microscopy (SECM) was successfully applied for the topographical imaging of live cells.^{29–31} The advantage of SECM based on a redox current as a feedback signal is that the working distance is longer than other feedback signals used for conventional SPMs. Furthermore, SECM is able to detect enzyme^{32–34} and cellular respiration^{35–37} activity and generate

^a Graduate School of Environmental Studies, Tohoku University, Aramaki Aoba 6-6-11-605, Sendai 980-8579.

E-mail: matsue@bioinfo.che.tohoku.ac.jp

^b Hokuto Denko Corporation, 3028 Uenohara, Kamiechi, Atsugi, Kanagawa 243-0801, Japan

^c Graduate School of Material Science, University of Hyogo, 3-2-1 Kouto, Kamigori-cho, Ako-gun, Hyogo 678-1297, Japan

^d Graduate School of Biomedical Engineering, Tohoku University, Sendai 980-8575

chemical reaction.^{38,39} However, the resolution of a typical SECM is inferior as compared to other SPMs because miniaturization of the electrode probe is very difficult. Some groups have used nanoelectrodes for live cell measurements.^{40,41} However, the nanoelectrodes were easily polluted, and therefore could only be used for a limited time.

The resolution of SICM depends on the size of pipette aperture. Since it is relatively easy to fabricate nanopipettes because of the simplicity of their structures, the resolution of SICM is high compared to SECM. In a previous study, a membrane protein was imaged by SICM using a pipette with a 15-nm diameter.⁴² The drawback of SICM is the fluctuations of ionic currents over time, which is called the DC drift. To circumvent this drift, a modulation mode⁸ and pulse mode^{43,44} were developed. However, an adequate probe scanning method has not been developed.

In this study, we adopted a standing approach (STA) mode in which the probe was moved vertically to first approach and then retracted from the sample surface at each measurement point on an *XY* plane during imaging. The STA mode is also useful for uneven substrates over a large range of scanning areas.^{45–49} The vertical motion of the pipette completely prevents contact with the sample surface. Furthermore, the DC drift in the probe current is completely nullified by defining the set point for the ionic current at each measurement point before the tip approaches the sample surface.

A major disadvantage of the STA mode is that the acquisition time for imaging is long compared to the conventional scanning mode. Therefore, the approach speed of the pipette was increased by adapting a field-programmable gate array (FPGA) board for feedback distance regulation. Korchev *et al.* very recently reported a similar concept for an SICM configuration for live cell imaging.⁵⁰ This novel SICM imaging algorithm will expand the applicability of SICM for characterizing various phenomena that occur on the surfaces and outside of live cells and tissues under truly stress-free physiological environments.

To evaluate the potential of the STA mode we imaged convoluted live cells and cell surfaces. The SICM setup used two scanning stages to obtain topographical images: wide-area scanning with micrometre resolution and narrow-area scanning with nanometre resolution. The resolution of SICM with the narrow-area scanning system was compared to that of AFM using a PDMS micro-mould. We investigated topographical imaging of MCF-7, HeLa and CHO cells, as well as myotubes formed in C2C12 cells and axons of a single PC12 cell. In addition, we also performed high speed (7 min per image) and high resolution imaging of live HeLa cells.

Experimental

Measurement system

The configuration of the scanning ion conductance microscopy (SICM) system used in the present study was essentially the same as the home-made SECM reported previously.⁴⁹ Electrochemical measurements used a two-electrode configuration with an Ag/AgCl (saturated KCl) reference electrode. The ionic current signal was amplified using a high-gain current

amplifier (Keithley, Model 427). The rise time of the current amplifier was set at 1–3 ms for high-speed ionic current feedback control. Optical images of the cells were observed using inverted optical microscopy (TE-300, Nikon) using an objective lens (CFI Fluor 20 \times , 0.45 NA, Nikon) and recorded with a digital camera (Coolpix 990, Nikon).

We used two scanning systems: wide-area and narrow-area scanning systems with minimum and maximum scan ranges from 100 \times 100 μm to 2000 \times 2000 μm and 5 \times 5 μm to 100 \times 100 μm , respectively. In the wide-area system, the pipette position was controlled by an *XYZ* stage (Suruga Seiki, K701-20R) driven by a stepping motor controller (Suruga Seiki, D70). The vertical position (*Z* direction) for the probe was precisely controlled by a piezoelectric actuator (Melles Griot, 17PAZ013) and an actuator controller (Melles Griot, 17PCZ001). The traversing distance of the stepping motor in the *XY* direction was 20 mm and that for the piezoelectric actuator in the *Z* direction was 80 μm . The system was controlled by a program written in Visual Basic 6.0 (Microsoft) using a 16-bit D/A converter board (Interface, PCI-3310) and 16-bit A/D converter board (Interface, PCI-3178). In the narrow area, a high resolution scanning system and a *XYZ* piezoelectric scanner (Physik Instrumente, P-517.3CL) connected to an amplifier module (Physik Instrumente, E-503.00) and servo control module (Physik Instrumente, E-509.C3) were used to precisely control the relative position of the probe and a sample. The system was controlled by a program written using LabVIEW 8.0 (National Instruments). Signals were converted to digital data using an FPGA board (NI-7831R, National Instruments). FPGA programming used a LabVIEW FPGA module that converted the LabVIEW programs into a very high-speed integrated circuit hardware description language (VHDL).

An AFM image was obtained in air using conventional AFM (NanoScope III AFM Dimension 3000 stage system; Digital Instruments, Inc., Santa Barbara, California) operated in a tapping mode.

Standing approach (STA) mode measurements

The STA mode featured repetitive approaches to and retractions from the surface by the probe for measurements while defining a new set point at each point. Fig. 1 shows a schematic diagram of the standing approach (STA) mode. The procedure is as follows: first, a reference ionic current was measured using a nanopipette positioned at a reference point (usually 2 μm from the sample surface). The set point was defined as 99% of the reference ionic current (Fig. 1(a)). Then, the nanopipette approached the surface at 20–100 nm ms^{−1} while monitoring the ionic current until the current was damped to the set point (Fig. 1(b)). The vertical position of the probe tip was also continuously monitored with the control system. Then, the nanopipette was retracted 2 μm upward to avoid contact with the surface during lateral movement (Fig. 1(c)). When the reference ionic current was less than 99.95% of the previous reference point, the probe was moved upward until the ionic current reached 99.95% of the previous reference point. Additionally, the probe was further retracted by 1 μm to avoid undesired

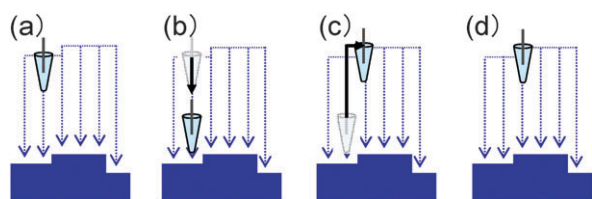


Fig. 1 Schematic representation of the standing approach mode. (a) The set point is established at a position far from the substrate. (b) Pipette engages the sample surface. (c) Pipette withdraws from the sample and moves to the next point. (d) The set point is re-established.

contact with the sample surface. A new set point was defined by measuring the reference ionic current (Fig. 1(d)).

Fabrication of nanopipette

The SICM nanopipettes were fabricated by pulling either a borosilicate glass pipette (id = 0.86 mm, od = 1.5 mm; GC150F-10, Harvard Apparatus) or a quartz glass pipette (id = 0.70 mm, od = 1.0 mm; Q100-70-7.5, Sutter Instrument). A borosilicate glass pipette was pulled using a capillary puller (Narishige PE-21). A quartz glass pipette was pulled using a carbon dioxide laser puller (Sutter Instruments, Model P-2000).

Fig. 2 shows SEM images of typical borosilicate and quartz nanopipettes. The inner/outer radii of borosilicate and quartz capillaries were 40/63 nm and 8/67 nm, respectively. We mainly used borosilicate nanopipettes for measurements.

Materials

D-(+)-Glucose, NaCl, KCl and $\text{Na}_2\text{SO}_4 \cdot 10\text{H}_2\text{O}$ were purchased from Wako Pure Chemicals (Osaka, Japan) and used without further purification. RPMI-1640 (Gibco), poly(dimethylsiloxane) (PDMS; Dow Corning Toray Co., Ltd.) and SU-8 (3050, Microchem) were purchased and used as received. All solutions were prepared using purified water from a Milli-Q II system (Millipore). PBS was prepared from 7.2 mM $\text{Na}_2\text{HPO}_4 \cdot 12\text{H}_2\text{O}$, 2.8 mM KH_2PO_4 and 150 mM NaCl (pH 7.0).

Fabrication of PDMS patterns

Line-and-space and hollow array patterns with PDMS were used to investigate the performance of the SICM system. These patterns were fabricated as follows: a 10:1 mixture of a silicon elastomer and curing agent was poured onto the masters on glass substrates and left at 80 °C for 1 h. After

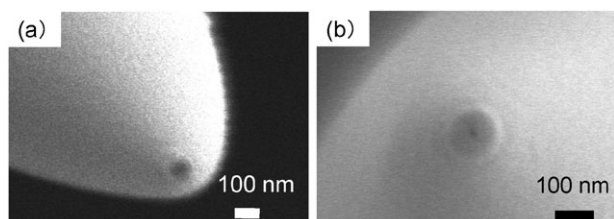


Fig. 2 Scanning electron microscopic photographs of (a) borosilicate and (b) quartz nanopipettes.

curing, the PDMS replica was peeled from the substrate. A line-and-space pattern was fabricated using a corresponding SU-8 master. The resulting pattern showed lines of width 80 and 100 μm and height 40 μm that were separated by 150 μm from adjacent lines. The master for the hollow array pattern was prepared by dispersing 500 nm diameter polystyrene beads (Polysciences Inc.) onto a glass substrate. The beads formed a densely-packed, self-assembled monolayer on the glass substrate after vaporizing the solution. The resulting substrate was used as the master for the hollow array pattern.

Cell cultures

HeLa cells (human cervix epithelial cell line), MCF-7 cells (human breast cell line) and CHO cells (Chinese hamster ovary cell line) were cultured in Petri dishes (Falcon) containing RPMI-1640 medium (Gibco) supplemented with 10% heat-inactivated fetal bovine serum (Gibco) and 1% penicillin–streptomycin (Gibco) at 37 °C under a 5% CO_2 atmosphere. C2C12 cells were cultured in DMEM (Gibco) supplemented with 10% FBS, 30 $\mu\text{g ml}^{-1}$ penicillin and 100 $\mu\text{g ml}^{-1}$ streptomycin (growth medium) at 37 °C under a 5% CO_2 atmosphere. Three days after plating, cells reached 80–90% confluence (day 0). C2C12 cell differentiation was then induced by switching the growth medium to DMEM supplemented with 2% calf serum, 30 $\mu\text{g ml}^{-1}$ penicillin and 100 $\mu\text{g ml}^{-1}$ streptomycin (differentiation medium). The differentiation medium was changed every 24 h. PC12 cells were cultured in Petri dishes (Falcon) using RPMI-1640 medium (Gibco) supplemented with 5 ng ml^{-1} nerve growth factor (7 s, Gibco), 10% heat-inactivated fetal bovine serum (Gibco) and 1% penicillin–streptomycin (Gibco) at 37 °C under a 5% CO_2 atmosphere. After 3 days of culturing, PC12 cells were attached to Petri dishes coated with collagen (Research Institute for the Functional Peptides) and differentiated by extending their axons.

Result

Imaging PDMS patterns

The development of micropipette-based live cell manipulation systems for inducing^{51,52} and collecting^{53,54} biomolecules and genes has been actively pursued. However, a process for precisely bringing a pipette probe to within the proximity of a cell surface remains difficult. An automated cell-surface recognition system with an XYZ positioner is required to improve manipulation efficiency and reliability. A feature of SICM is the possibility of obtaining sub-micro scale topographic images under physiological conditions.

To test the performance of the wide-area scanning system, a PDMS micro-mould with line patterns was imaged in 100 mM KCl (Fig. 3(a) and (b)). The 2D and 3D topographic images indicated clear patterns of 80 and 100- μm wide lines (dark) and 150- μm wide spaces (bright). The height was 30 μm . These dimensions agreed well with those observed using a conventional optical microscope. The topography of HeLa cells was also imaged using the same system in RPMI-1640 medium (Fig. 3(c)). The height of HeLa cells calculated from

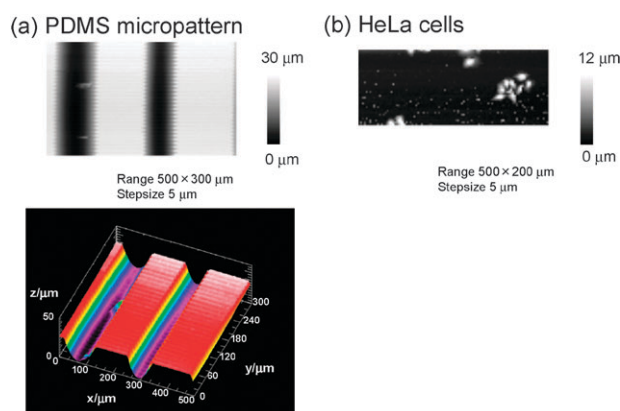


Fig. 3 SICM topographic images of (a) linear pattern PDMS and (b) HeLa cells in 100 mM KCl and RPMI-1640 medium, respectively. SICM pipette aperture = 100 nm. Applied voltage = -20 mV vs. Ag/AgCl. Step size = 5 μ m. Scan ranges were 500×300 μ m and 500×200 μ m, respectively.

the image was 11 μ m, which was in good agreement with the results obtained by high resolution SICM with the narrow-area scanning system, as shown later.

The performance of SICM using a high resolution scanning system was investigated using a hollow-array PDMS pattern in the STA mode. Fig. 4 shows the images of the patterns obtained using SICM and AFM systems. The SICM image was very similar to the AFM image showing the periodic nanostructure on the PDMS surface. From the cross-section of the SICM image, the height and inter-space of the nanostructure were found to be 120 – 130 nm and 540 – 600 nm, respectively, which were also in good agreement with those obtained from the AFM image. The resolution of SICM was defined by the pipette inner radius, in this experiment 40 nm, therefore a SICM image was laterally distorted compared with an AFM image. However the resolution can improve by using a small pipette and these results clearly indicate that SICM using an STA mode can be applied to investigate nanostructures in solution.

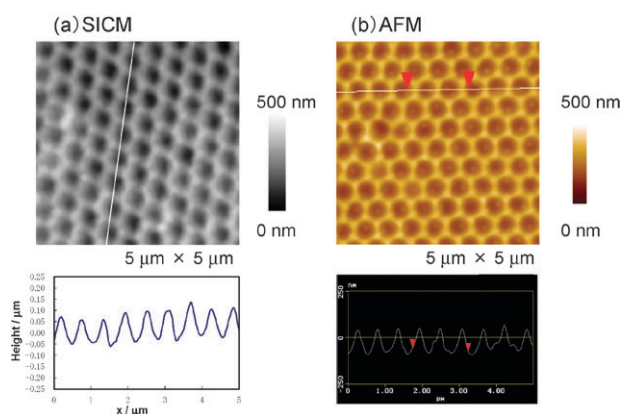


Fig. 4 (a) SICM and (b) AFM topographic images and cross-sections of a PDMS surface moulded by self-assembled 500 -nm diameter beads. SICM pipette aperture = 100 nm. Applied voltage = -300 mV vs. Ag/AgCl. Step size = 50 nm. Imaged in 100 mM KCl. AFM measurements were performed in air. Scan range was 5×5 μ m.

Live cell imaging by SICM

We also investigated the imaging of different types of live cells using the high resolution SICM system. Fig. 5 shows the topographic images of HeLa, CHO, MCF-7 and C2C12 cells in culture media. The images clearly show cell features without artifacts. The heights of MCF-7, HeLa and CHO cells were 10 , 9 and 9 μ m, respectively. In a previous paper, shear-force distance regulation was used to image live cell topography, although it was difficult to obtain a clear shear force signal from the cell if the solution viscosity was high. Therefore, we believe that SICM is a suitable system for live cell topography measurements because solution viscosity does not affect ionic currents. Furthermore, the feedback signal from an ionic current can be easily amplified by increasing the applied voltage between the electrodes in the pipette and bath. From the 3D image, the differences in curvatures of HeLa and CHO cells were clearly distinguished. The SICM images of C2C12 cells clearly demonstrate myotubes inside the cells, whereas they are unclear and difficult to recognize in optical microscopy images.

The STA mode was effective for topographic imaging of a convoluted structure. Fig. 6(a)–(c) shows SICM optical and topographic images of a single PC12 cell and its axons. The heights of the axon and cell body calculated from the 3D image were 2 – 4 μ m and 18 – 20 μ m, respectively. Fig. 6(d) shows a histogram of the differences in height between two adjacent pixels in the SICM image. The occupancy rate of the height differences less than 0.3 μ m is 64% ; this flat area corresponds to the substrate surface. The intermediate range between 0.3 and 2.1 μ m comprises 31% , probably indicating cell surface area. The third category with height differences of more than 2.1 μ m shows the edges of the cell body and axons.

Fig. 6(e) shows the SICM images after extracting the pixels of the above three categories indicating the substrate area, cell and axon surfaces, and edges (or outlines). The STA mode is absolutely superior to the conventional lateral scanning mode when capturing images of fragile and rough surfaces. As another advantage, the STA mode can define the set point at each measurement point before the pipette approaches the sample. Therefore, the DC drift is not a serious problem and a clear topographic image can be acquired, although the level of ionic current changed by at most 7 nA during this imaging.

Increase imaging speed

The SICM in the STA mode was useful for imaging the topographies of live cells. However, the imaging time in the STA mode was longer than the conventional lateral scanning mode because of the time-consuming algorithm for the repeated vertical motions of the probe. Especially, concerning the cell imaging on the whole, the nanopipette should approach the surface and then move upward at least 6 μ m before going to the next XY measurement point to avoid undesired contact with the sample surface, because of the drastic height change at the edge of the living cell (Fig. 6(d)). We accelerated the vertical and lateral movement speeds by introducing an FPGA board and high speed algorithm.

Fig. 7 shows the conventional STA mode and high-speed mode images of live MCF-7 cells in RPMI-1640 solution with

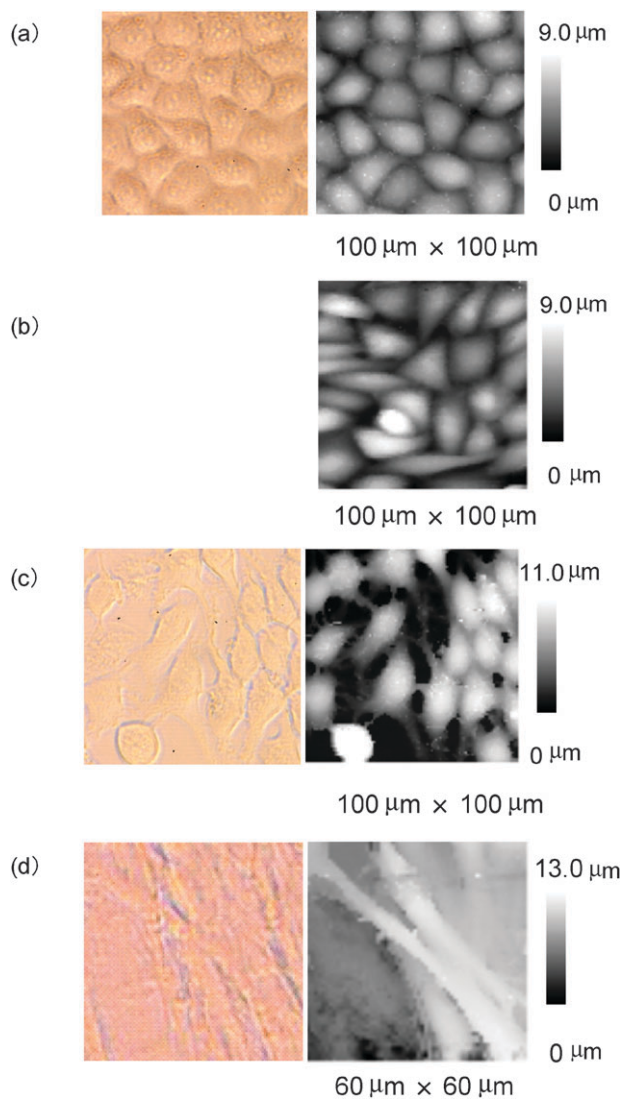


Fig. 5 Photograph (left) and SICM topographic images (right) of (a) HeLa, (b) CHO, (c) MCF-7 and (d) C2C12 cells. Pipette aperture = 100 nm. Applied voltage = -20 mV vs. Ag/AgCl. Step size = 1 μ m. Scan range areas were 100×100 μ m, 100×100 μ m and 60×60 μ m, respectively. Cells were plated on Petri dishes and imaged in growth medium.

a scan area of 100×100 μ m, a step size of 0.78 μ m and 16 384 data points. These images showed good agreement and heights were the same as in the result of Fig. 5(c). FPGA is a device that contains a matrix of reconfigurable gate array logic circuitry. It can perform complex and discrete signal processing algorithms with clock rates at a maximum of 40 MHz. The probe-sample distance feedback control and data acquisition can be achieved without completing the main PC operation. The high speed algorithm enables minimizing the probe upward distance, in this case 1.2 μ m, and avoiding the deformation of the living cells by comparing a reference current with the previous one and moving the probe upward when the probe contacts with a cell during lateral movement. The entire imaging time of the high speed algorithm required was 450 s with each measurement point of 27 ms. By comparison, the conventional STA mode imaging required 965 s for

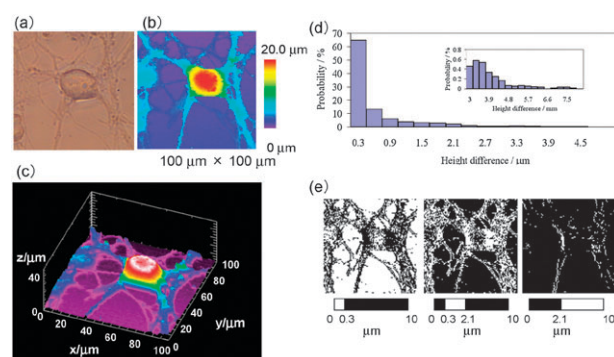


Fig. 6 Photograph (a) and SICM topographic 2D (b) and 3D (c) images of a PC12 cell. (d) Histogram of the probability of the pixels as a function of the height difference as the tip moved to the next pixel. (e) Pixel distributions for varying ranges of the height differences. Pipette aperture = 100 nm. Applied voltage = -20 mV vs. Ag/AgCl. Scan range was 100×100 μ m and step size = 1 μ m. Cells were plated on Petri dishes and imaged in growth medium.

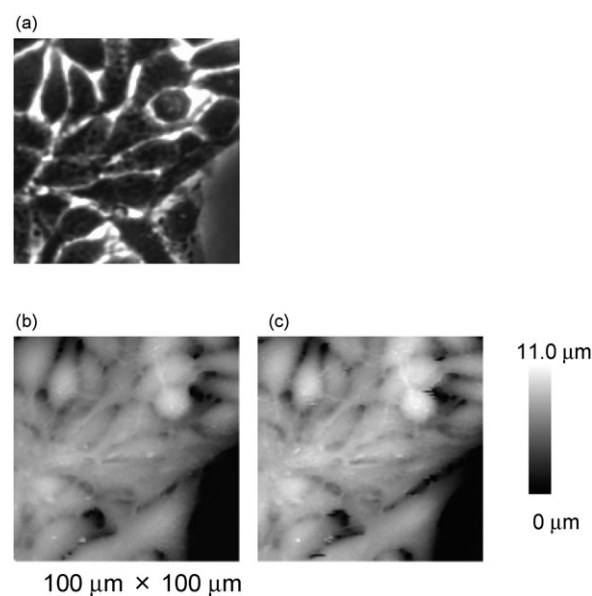


Fig. 7 Photograph (a) and SICM topography of STA mode (b) and high speed mode (c) topography images of MCF-7 cells. The pipette aperture = 100 nm. Applied voltage = -300 mV. The scan range = 100×100 μ m, and the step size = 0.78 μ m.

imaging the same area. Adopting the FPGA board and high speed algorithm accomplished increasing the imaging speed.

Conclusions

SICM with an STA mode was successfully applied to 2D and 3D imaging of live cells without cell contact and cell shape deformation. Both the wide-area and high-resolution scanning systems gave quantitative information on cell structures. Furthermore, DC drifts in the pipette currents were completely nullified by defining the ionic current of each set point before the probe tip approached a cell. Longer image acquisition time, which was the major drawback of this mode, was circumvented by improving the scanning speed after including an FPGA board and high-speed imaging algorithm. This

scanning method will extend the research fields applicable to SICM and enhance the understanding of the phenomena involved in morphological changes in cells.

Acknowledgements

This work was supported in part by a Grant-in-Aid for Scientific Research (18101006) from MEXT (Ministry of Education, Culture, Sports, Science and Technology), Japan and Grants-in-Aid for Collaborative Development of Innovative Seeds from Japan Science and Technology Agency. Y.T. acknowledges the support of a research fellowship from the Japan Society for the Promotion of Science. We also acknowledge Atsushi Kamoshida from National Instruments for the support to construct the program for controlling the SICM system.

Notes and references

- D. J. Muller and Y. F. Dufrene, *Nat. Nanotechnol.*, 2008, **3**, 261.
- R. Garcia and R. Perez, *Surf. Sci. Rep.*, 2002, **47**, 197.
- T. Ando, N. Koderia, E. Takai, D. Maruyama, K. Saito and A. Toda, *Proc. Natl. Acad. Sci. U. S. A.*, 2001, **98**, 12468.
- P. K. Hansma, B. Drake, O. Marti, S. A. C. Gould and C. B. Prater, *Science*, 1989, **243**, 641.
- Y. E. Korchev, C. L. Bashford, M. Milovanovic, I. Vodyanoy and M. J. Lab, *Biophys. J.*, 1997, **73**, 653.
- Y. E. Korchev, M. Milovanovic, C. L. Bashford, D. C. Bennett, E. V. Sviderskaya, I. Vodyanoy and M. J. Lab, *J. Microsc.*, 1997, **188**, 17.
- M. A. Edwards, C. G. Williams, A. L. Whitworth and P. R. Unwin, *Anal. Chem.*, 2009, **81**, 4482.
- A. I. Shevchuk, J. Gorelik, S. E. Harding, M. J. Lab, D. Klenerman and Y. E. Korchev, *Biophys. J.*, 2001, **81**, 1759.
- Y. E. Korchev, M. Raval, M. J. Lab, J. Gorelik, C. R. W. Edwards, T. Rayment and D. Klenerman, *Biophys. J.*, 2000, **78**, 2675.
- A. M. Rothery, J. Gorelik, A. Bruckbauer, W. Yu, Y. E. Korchev and D. Klenerman, *J. Microsc.*, 2003, **209**, 94.
- A. Mannelquist, H. Iwamoto, G. Szabo and Z. Shao, *J. Microsc.*, 2002, **205**, 53.
- A. Mannelquist, H. Iwamoto, G. Szabo and Z. F. Shao, *Appl. Phys. Lett.*, 2001, **78**, 2076.
- A. I. Shevchuk, P. Hobson, M. J. Lab, D. Klenerman, N. Krauzewicz and Y. E. Korchev, *Pfluegers Arch.*, 2008, **456**, 227.
- A. I. Shevchuk, P. Hobson, M. J. Lab, D. Klenerman, N. Krauzewicz and Y. E. Korchev, *Biophys. J.*, 2008, **94**, 4089.
- J. Gorelik, A. Shevchuk, M. Ramalho, M. Elliott, C. Lei, C. F. Higgins, M. J. Lab, D. Klenerman, N. Krauzewicz and Y. Korchev, *Proc. Natl. Acad. Sci. U. S. A.*, 2002, **99**, 16018.
- A. Bruckbauer, L. M. Ying, A. M. Rothery, D. J. Zhou, A. I. Shevchuk, C. Abell, Y. E. Korchev and D. Klenerman, *J. Am. Chem. Soc.*, 2002, **124**, 8810.
- L. M. Ying, A. Bruckbauer, A. M. Rothery, Y. E. Korchev and D. Klenerman, *Anal. Chem.*, 2002, **74**, 1380.
- A. Bruckbauer, D. J. Zhou, L. M. Ying, Y. E. Korchev, C. Abell and D. Klenerman, *J. Am. Chem. Soc.*, 2003, **125**, 9834.
- L. M. Ying, S. S. White, A. Bruckbauer, L. Meadows, Y. E. Korchev and D. Klenerman, *Biophys. J.*, 2004, **86**, 1018.
- L. M. Ying, A. Bruckbauer, D. J. Zhou, J. Gorelik, A. Shevchuk, M. Lab, Y. Korchev and D. Klenerman, *Phys. Chem. Chem. Phys.*, 2005, **7**, 2859.
- J. D. Piper, R. W. Clarke, Y. E. Korchev, L. M. Ying and D. Klenerman, *J. Am. Chem. Soc.*, 2006, **128**, 16462.
- K. T. Rodolfa, A. Bruckbauer, D. J. Zhou, A. I. Shevchuk, Y. E. Korchev and D. Klenerman, *Nano Lett.*, 2006, **6**, 252.
- J. D. Piper, C. Li, C. J. Lo, R. Berry, Y. Korchev, L. M. Ying and D. Klenerman, *J. Am. Chem. Soc.*, 2008, **130**, 10386.
- J. Gorelik, Y. C. Gu, H. A. Spohr, A. I. Shevchuk, M. J. Lab, S. E. Harding, C. R. W. Edwards, M. Whitaker, G. W. J. Moss, D. C. H. Benton, D. Sanchez, A. Darszon, I. Vodyanoy, D. Klenerman and Y. E. Korchev, *Biophys. J.*, 2002, **83**, 3296.
- Y. C. Gu, J. Gorelik, H. A. Spohr, A. Shevchuk, M. J. Lab, S. E. Harding, I. Vodyanoy, D. Klenerman and Y. E. Korchev, *FASEB J.*, 2002, **16**, 748.
- A. K. Dutta, Y. E. Korchev, A. I. Shevchuk, S. Hayashi, Y. Okada and R. Z. Sabirov, *Biophys. J.*, 2008, **94**, 1646.
- Y. E. Korchev, Y. A. Negulyaev, C. R. W. Edwards, I. Vodyanoy and M. J. Lab, *Nat. Cell Biol.*, 2000, **2**, 616.
- F. Moreno-Herrero, J. Colchero, J. Gomez-Herrero and A. M. Baro, *PhRvE*, 2004, **69**, 031915.
- R. T. Kurulugama, D. O. Wipf, S. A. Takacs, S. Pongmayteegul, P. A. Garriss and J. E. Baur, *Anal. Chem.*, 2005, **77**, 1111.
- Y. Hirano, Y. Nishimiya, K. Kowata, F. Mizutani, S. Tsuda and Y. Komatsu, *Anal. Chem.*, 2008, **80**, 9349.
- L. P. Bauermann, W. Schuhmann and A. Schulte, *Phys. Chem. Chem. Phys.*, 2004, **6**, 4003.
- Y. Takahashi, T. Miyamoto, H. Shiku, R. Asano, T. Yasukawa, I. Kumagai and T. Matsue, *Anal. Chem.*, 2009, **81**, 2785.
- H. Shiku, T. Matsue and I. Uchida, *Anal. Chem.*, 1996, **68**, 1276.
- G. Wittstock, K. J. Yu, H. B. Halsall, T. H. Ridgway and W. R. Heineman, *Anal. Chem.*, 1995, **67**, 3578.
- H. Shiku, T. Shiraishi, H. Ohya, T. Matsue, H. Abe, H. Hoshi and M. Kobayashi, *Anal. Chem.*, 2001, **73**, 3751.
- T. Yasukawa, T. Kaya and T. Matsue, *Anal. Chem.*, 1999, **71**, 4637.
- Y. S. Torisawa, T. Kaya, Y. Takii, D. Oyamatsu, M. Nishizawa and T. Matsue, *Anal. Chem.*, 2003, **75**, 2154.
- H. Shiku, T. Takeda, H. Yamada, T. Matsue and I. Uchida, *Anal. Chem.*, 1995, **67**, 312.
- H. Kaji, K. Tsukidate, T. Matsue and M. Nishizawa, *J. Am. Chem. Soc.*, 2004, **126**, 15026.
- P. Sun, F. O. Laforge, T. P. Abeyweera, S. A. Rotenberg, J. Carpino and M. V. Mirkin, *Proc. Natl. Acad. Sci. U. S. A.*, 2008, **105**, 443.
- B. B. Katemann and T. Schuhmann, *Electroanalysis*, 2002, **14**, 22.
- A. I. Shevchuk, G. I. Frolenkov, D. Sanchez, P. S. James, N. Freedman, M. J. Lab, R. Jones, D. Klenerman and Y. E. Korchev, *Angew. Chem., Int. Ed.*, 2006, **45**, 2212.
- P. Happel, G. Hoffmann, S. A. Mann and I. D. Dietzel, *J. Microsc.*, 2003, **212**, 144.
- S. A. Mann, G. Hoffmann, A. Hengstenberg, W. Schuhmann and I. D. Dietzel, *J. Neurosci. Methods*, 2002, **116**, 113.
- H. Yamada, H. Fukumoto, T. Yokoyama and T. Koike, *Anal. Chem.*, 2005, **77**, 1785.
- H. Yamada, Y. Ikuta, T. Koike and T. Matsue, *Chem. Lett.*, 2008, **37**, 392.
- H. Yamada, M. Ogata and T. Koike, *Langmuir*, 2006, **22**, 7923.
- Y. Takahashi, Y. Hirano, T. Yasukawa, H. Shiku, H. Yamada and T. Matsue, *Langmuir*, 2006, **22**, 10299.
- Y. Takahashi, H. Shiku, T. Murata, T. Yasukawa and T. Matsue, *Anal. Chem.*, 2009, **81**, 9674.
- P. Novak, C. Li, A. I. Shevchuk, R. Stepanyan, M. Caldwell, S. Hughes, T. G. Smart, J. Gorelik, V. P. Ostanin, M. J. Lab, G. W. Moss, G. I. Frolenkov, D. Klenerman and Y. E. Korchev, *Nat. Methods*, 2009, **6**, 279.
- F. O. Laforge, J. Carpino, S. A. Rotenberg and M. V. Mirkin, *Proc. Natl. Acad. Sci. U. S. A.*, 2007, **104**, 11895.
- H. Matsuoaka, T. Komazaki, Y. Mukai, M. Shibusawa, H. Akane, A. Chaki, N. Uetake and M. Saito, *J. Biotechnol.*, 2005, **116**, 185.
- Y. Nashimoto, Y. Takahashi, T. Yamakawa, Y. S. Torisawa, T. Yasukawa, T. Ito-Sasaki, M. Yokoo, H. Abe, H. Shiku, H. Kambara and T. Matsue, *Anal. Chem.*, 2007, **79**, 6823.
- H. Shiku, T. Yamakawa, Y. Nashimoto, Y. Takahashi, Y. Torisawa, T. Yasukawa, T. Ito-Sasaki, M. Yokoo, H. Abe, H. Kambara and T. Matsue, *Anal. Biochem.*, 2009, **385**, 138.